Supporting Information

Aperture Control in Polymer-based Composites with Hybrid Core-Shell Spheres for Frequency-Selective Electromagnetic Interference Shielding

Uiseok Hwang,[a] Junyoung Kim,[b] Hanna Sun,[b] In-Kyung Park,[a] Jonghwan Suhr,[c] and Jae-Do Nam[ab]*

[a]Department of Polymer Science and Engineering, Sungkyunkwan University, Suwon 16419, Republic of Korea
[b]Department of Energy Science, Sungkyunkwan University, Suwon 16419, Republic of Korea
[c]School of Mechanical Engineering, Sungkyunkwan University, Suwon 16419, Republic of Korea
*Corresponding author E-mail: jdnam@skku.edu

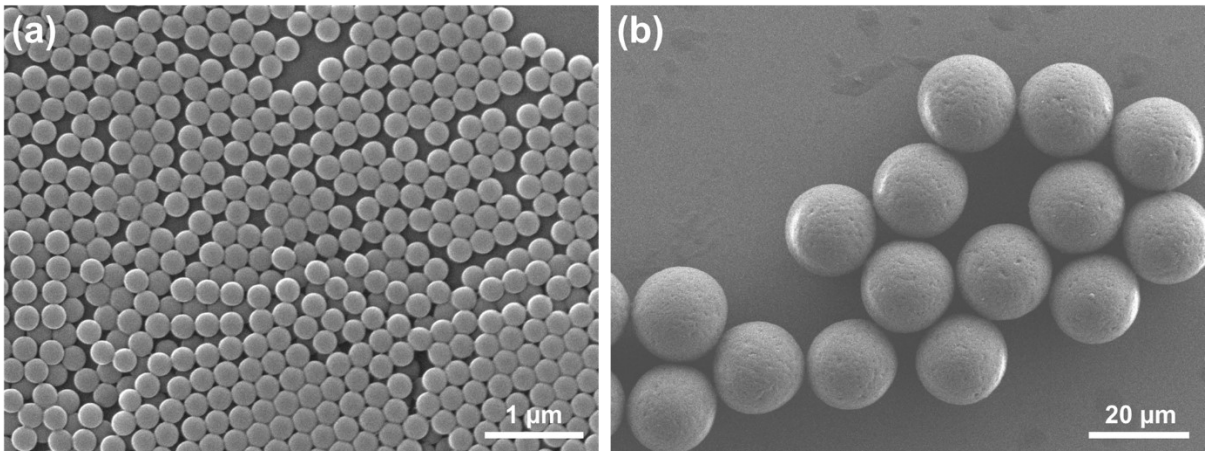

Fig. S1. FE-SEM images of PS and PMMA microspheres with average diameters of 200 nm and 20 μm, which were served as core materials for the Graphene@PS and Ni/Au@PMMA core-shell spheres, respectively.

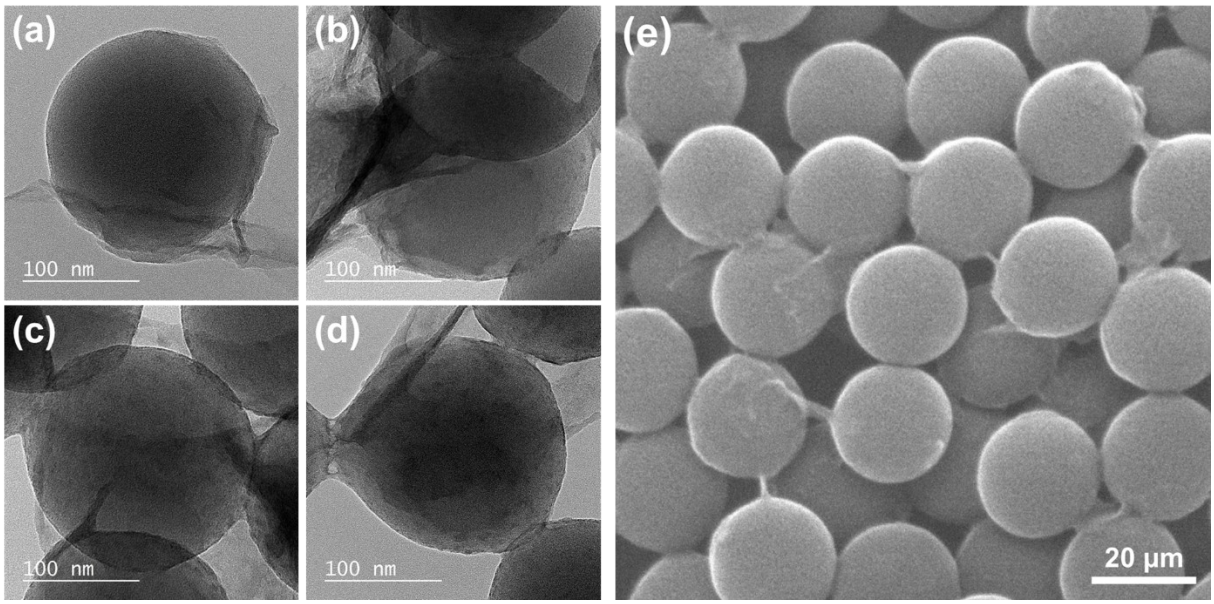

Fig. S2. (a–d) HRTEM images and (e) FE-SEM image of the Graphene@PS spheres.

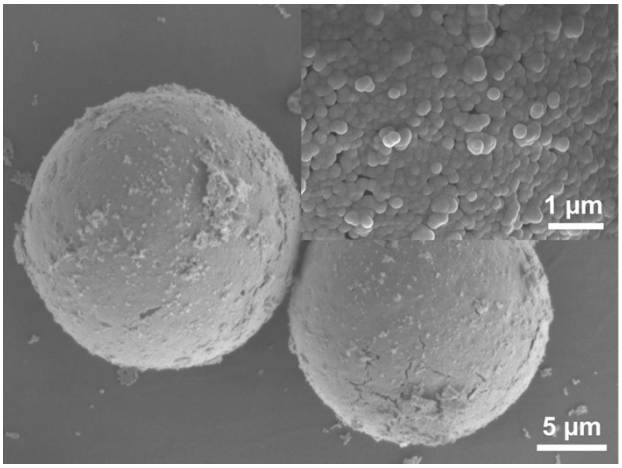

Fig. S3. FE-SEM images of Ni@PMMA spheres at different magnifications.

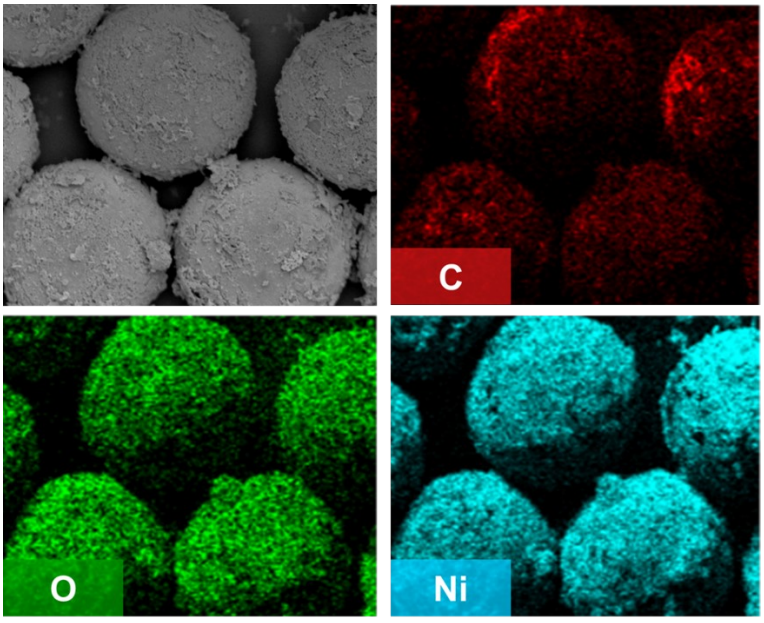

Element	Wt.%	Atomic %
C	7.33	23.43
O	9.13	21.92
Ni	83.54	54.65

Fig. S4. EDS elemental mapping images and composition table of Ni@PMMA spheres showing the distribution of elements (C, O, and Ni).

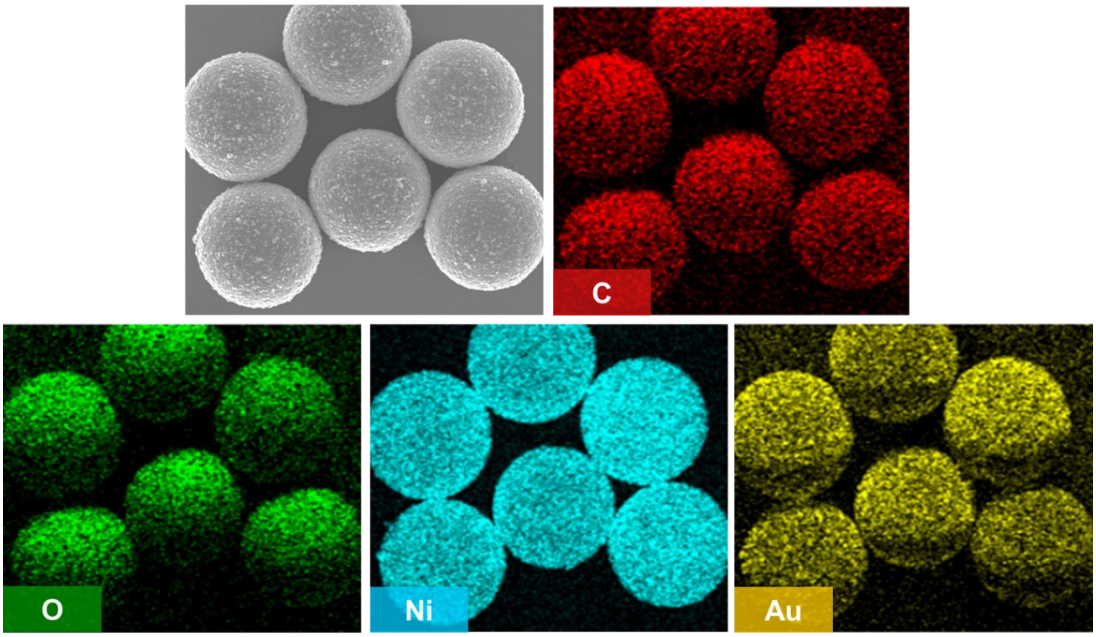

Element	Wt.%	Atomic %
C	16.44	47.87
O	4.54	9.91
Ni	67.42	40.17
Au	11.61	2.06

Fig. S5. EDS elemental mapping images and composition table of Ni/Au@PMMA spheres showing the distribution of elements (C, O, Ni, and Au).

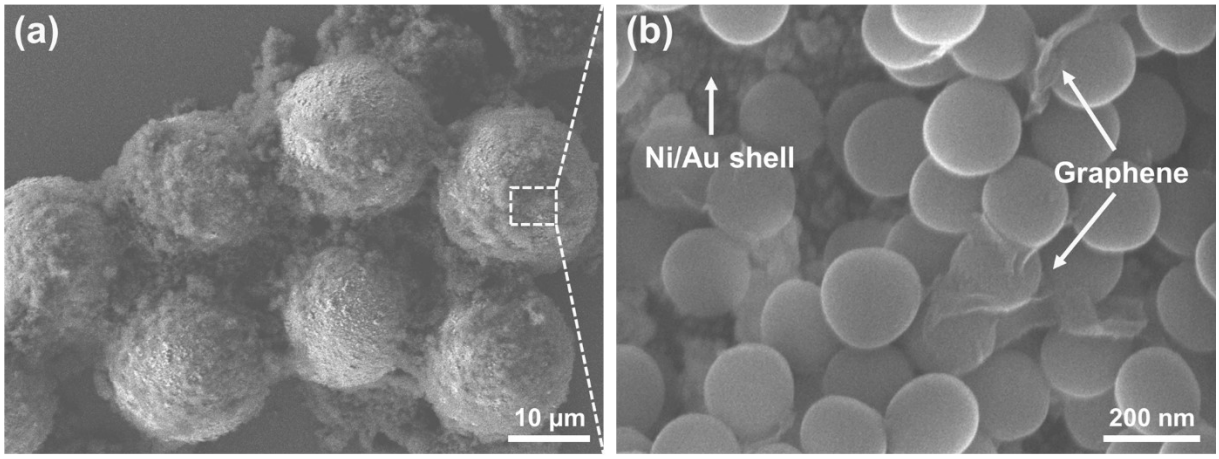

Fig. S6. FE-SEM images of Ni/Au@PMMA and Graphene@PS spheres mixed in a weight ratio of 5:2 at different magnifications.

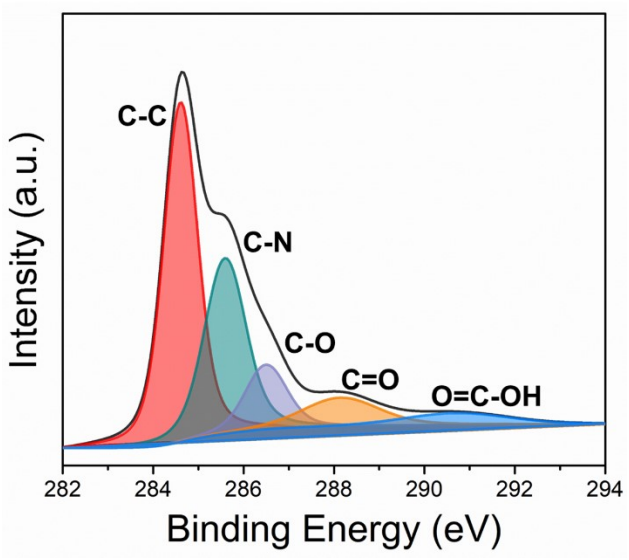

Fig. S7. XPS C1s core-level spectra of PPD-reduced graphene oxide sheets.

Table S1. Weight composition, electrical conductivity, and EMI SE of various core-shell sphere composites.

Composite	Weight fraction (wt.%)						Electrical conductivity (S/m)	EMI SE (dB)
	Graphene	PS	Nickel	Gold	PMMA	DGEBA		
G70	1.43	68.57	0	0	0	30	–	1.8
M40	0	0	7.61	0.54	31.84	60	–	17.8
M50	0	0	9.52	0.68	39.81	50	0.0226	36.8
M60	0	0	11.42	0.82	47.77	40	12,183	55.7
M70	0	0	13.32	0.95	55.73	30	14,768	87.4
M10/G60	1.23	58.77	1.90	0.14	7.96	30	–	2.8
M20/G50	1.02	48.98	3.81	0.27	15.92	30	–	3.8
M30/G40	0.82	39.18	5.71	0.41	23.88	30	–	5.8
M40/G30	0.61	29.39	7.61	0.54	31.84	30	–	12.3
M50/G20	0.41	19.59	9.52	0.68	39.81	30	–	11.3
M60/G10	0.20	9.80	11.42	0.82	47.77	30	4,831	96.5

*The electrical conductivities of the samples that are not mentioned were <0.0005 S/m.

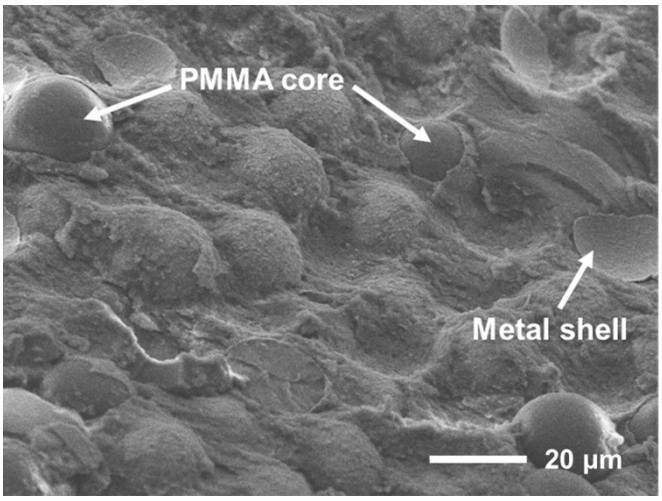

Fig. S8. Cross-sectional FE-SEM image of the M60/G10 composite. Partially exposed PMMA cores with smooth surfaces and broken metal shells that were separated from the Ni/Au@PMMA spheres could be observed, clearly showing the core-shell structure of the particles. The Graphene@PS spheres were relatively difficult to find in the figure, which indicated that the spheres were well-dispersed among the Ni/Au@PMMA spheres in the epoxy resin.

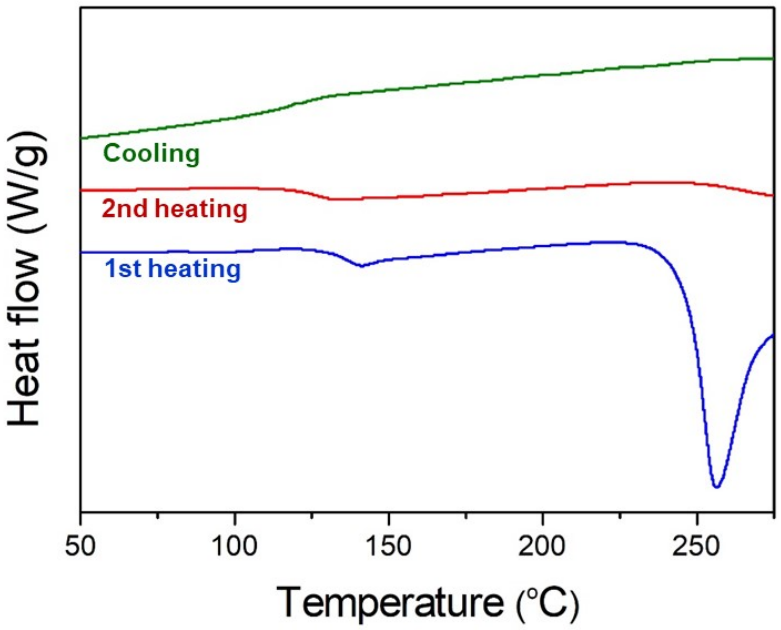

Fig. S9. DSC thermal cycles for PMMA microspheres. In the first heating process, there were two transitions, while in the subsequent cooling process, there was only one transition at about the same temperature range. The first transition in the first heating curve was identified as the glass transition. In the second heating process, the second transition observed in the first heating curve disappeared. Since PMMA is a typical amorphous polymer, the second transition observed in the first heating curve should be related to the presence of additional chemicals. According to the DSC result of the second thermal cycle, the glass transition temperature (T_g) of the PMMA microsphere was determined as 125°C.

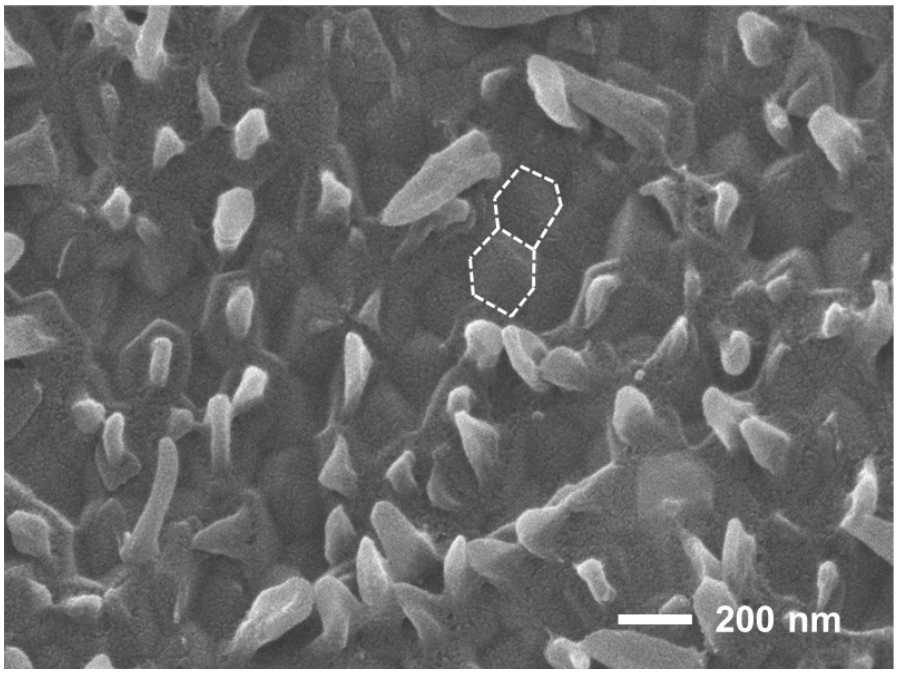

Fig. S10. Cross-sectional FE-SEM image of the M10/G60 composite. When the composite was compression-molded at 100℃, which is near glass-transition temperature of PS, the Graphene@PS spheres were compressed into clusters, showing deformed structure of hexagonal blocks (white dash) with some protuberances on each block.

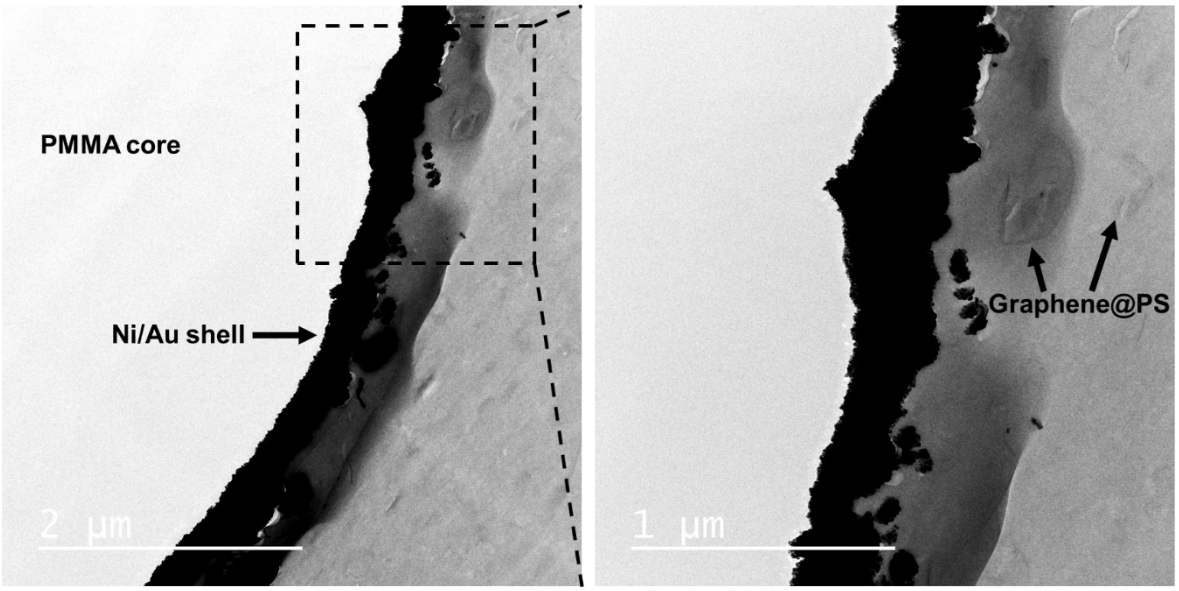

Fig. S11. HRTEM images of ultrathin section of M30/G40 composite at different magnifications.

Table S2. Comparison of average reflection, absorpiotn, and transmission fractions of different core-shell sphere composites in the X-band frequency range.

Composites	Shielding mechanisms (%)		
	Reflection	Absorption	Transmission
G70	12.0	21.4	66.6
M60	92.3	7.7	2.7×10^4
M70	92.0	8.0	1.8×10^7
M60/G10	90.2	9.8	2.3×10^8

Table S3. Frequency-selective EMI shielding properties of various hybrid core-shell sphere composites.

Composites	f_s (GHz)	A_{max} (%)	A_{min} (%)	α (A_{max}/A_{min})
M10/G60	10.65	32.3	16.8	1.92
M20/G50	9.05	24.4	17.2	1.42
M30/G40	12.05	24.7	15.6	1.58
M40/G30	12.4	31.1	22.5	1.38
M50/G20	12.4	21.9	9.7	2.26
M60/G10	10.05	18.6	4.1	4.54
M10/G60+G70	10.6	53.5	24.1	2.21
M20/G50+G70	10.15	60.8	27.6	2.20
M30/G40+G70	9.9	59.7	32.2	1.85
M40/G30+G70	9.6	69.1	46.3	1.49
M50/G20+G70	8.75	58.1	47.3	1.23
M60/G10+G70	11.3	76.1	30.0	2.82

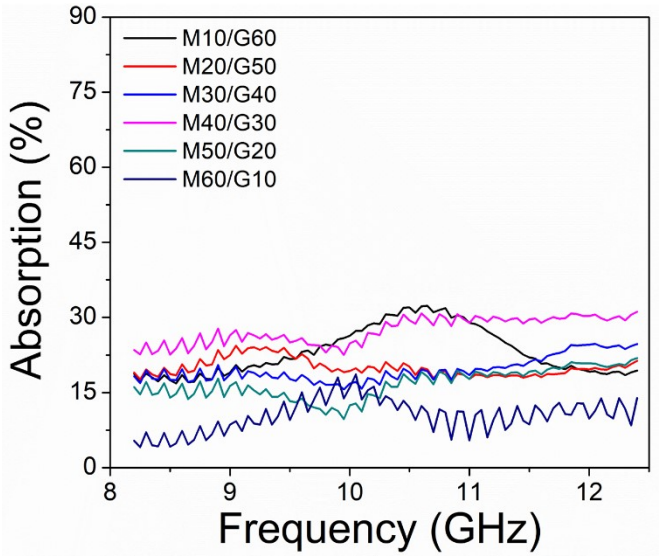

Fig. S12. Absorption fraction of the M00/G00 composites as a function of frequency.

Table S4. EMI shielding performance of various conductive polymer composites.

Filler	Matrix	Content (wt.%)	EMI SE (dB)			Thickness (mm)	Frequency range (GHz)	Ref.
			SE_T	SE_A	SE_R			
Ni/Au (M70)	PMMA, Epoxy	14.27	87.4	76.4	10.9	1	8.2–12.4	This work
RGO/Ni/Au (M60/G10)	PS, PMMA, Epoxy	12.44	96.5	86.4	10.1	1	8.2–12.4	
RGO/Ni/Au (M60/G10+G70)	PS, PMMA, Epoxy	6.94	70.8	65.1	5.7	2	8.95	
			67.0	62.9	4.1		10.0	
			67.4	66.2	1.2		11.3	
			69.0	66.3	2.7		12.4	
RGO	PEI	10	22.5	19.66	2.84	2.3	8–12	[1]
RGO	PS	30	29	27.7	1.3	2.5	8.2–12.4	[2]
RGO	WPU	5*	26	24	2	2	8.2–12.4	[3]
RGO	WPU	7.5	34	31	3	1	8.2–12.4	[4]
RGO	PS	3.47*	41.4	38.4	3	2.5	8.2–12.4	[5]
RGO	PEDOT-PSS	25	67.3	65.3	2	0.8	8.2–12.4	[6]
RGO	PP	20	51	43	8	2	8–18	[7]
GO	PMMA	1.8*	19	18	1	2.4	8–12	[8]
3D graphene	PDMS	0.8	23	19	4	1	8–12	[9]
S-doped RGO	PS	7.5*	21	17.3	3.7	2	12.4–18	[10]
Aligned GO foam	Epoxy	0.8	33	29	4	4	8–12	[11]
Carbon nanowires/graphene	PDMS	25.3	36	25	11	1.6	8.2–12.4	[12]
Pristine graphene	PI	50	54.11	34.94	19.17	0.04	8.2–12.4	[13]
MWCNT	PLLA	10	24.6	23.8	0.8	2.5	8.0–12.4	[14]
MWCNT	PC	5	25	20	5	1.85	8.2–12.4	[15]
MWCNT	PP	7.5*	36.4	29.1	7.3	1	8–12	[16]
MWCNT	WPU	7*	49	41	8	4.5	8.2–12.4	[17]
SWCNT	PS	7	20	12.79	7.21	/	8.2–12.4	[18]
SWCNT	Epoxy	15	16.99	6.99	10	1.5	0.5–1.5	[19]
CNT sponge	Epoxy	2	44	38	5	2	8–12	[20]
MWCNT	WPU	76.2	62	46.5	15.5	0.5	8.2–12.4	[21]
MWCNT	PEDOT	15	66	58	8	2.8	12.4–18	[22]
MWCNT	Coal tar	25	56	49	7	0.6	8.2–12.4	[23]
Carbon black	SEBS	15	17.57	12.69	4.88	5	8.2–12.4	[24]
Graphite	PE	7.05*	35.8	32.5	3.3	2.5	8.2–12.4	[25]
Graphite	ABS	15	56	48	8	3	8–12	[26]
CNF	ABS	15	27.6	20.6	7	1.1	8.2–12.4	[27]
Carbon fiber	PP	10*	24.9	20.17	4.73	3.2	8.2–12.4	[28]
Carbon fiber/Fe_3O_4	Epoxy	20	17.5	16.5	1	13	1–18	[29]

Carbon fiber/Fe_3O_4	PDMS	5	67.9	55.47	12.43	0.7	8.2–12.4	[30]
RGO/Fe_3O_4	PVC	10	12.5	4	8.5	1.8	8.2–12.0	[31]
RGO/Fe_3O_4	PS	2.24*	35	31.5	3.5	/	8–12	[32]
RGO/γ-Fe_2O_3	PANI	75	65	55	10	2.5	8.2–12.4	[33]
Ag nanowires	PS	2.5*	63.2	57.1	6.1	0.8	8.2–12.4	[34]
Cu nanowires	PS	2.1*	34	18	16	0.2	8.2–12.4	[35]
Ni fiber	PES	7*	87	72	15	2.85	1–2	[36]
Ag nanowires	PANI	11*	37.7	26.9	10.8	0.0117	8.2–12.4	[37]
Cu/Graphite	PVC	20	68	57	11	2	1–20	[38]
$Ti_3C_2T_x$	PS	1.9*	61.2	54.7	6.5	2	8.2–12.4	[39]
$Ti_3C_2T_x$	SA	60	40	23	17	0.008	8.2–12.4	[40]
$Ti_3C_2T_x$	Wax	90	76.1	67.3	8.8	1	8.2–12.4	[41]
RGO/$Ti_3C_2T_x$	Epoxy	0.99*	56.4	50.7	5.7	2	12.4	[42]
Ni ferrite	PVDF	50*	67	54	13	2	8.2–12.4	[43]

* - vol.%

RGO: Reduced graphene oxide; PS: Polystyrene; PMMA: Poly(methyl methacrylate); PEI: Poly(ether imide); WPU: Waterborne polyutrethane; PEDOT: Poly(3,4-ethylenedioxy-thiophene); PSS: Poly(styrenesulfone); PP: Polypropylene; PDMS: Polydimethylsilane; PI: Polyimide; MWCNT: Multi-walled carbon nanotube; SWCNT: Single-walled carbon nanotube; PLLA: Poly-L-lactic acid; PC: Polycarbonate; SEBS: Styrene-ethylene-butylene-styrene; PE: Polyethylene; ABS: Acrylonitrile butadiene styrene; CNF: Carbon nanofiber; PVC: Poly(vinyl chloride); PES: Poly(ether sulfone); PANI: Polyanilie; SA: Sodium alginate; PVDF: Poly(vinylidene fluoride).

Note S1: EMI shielding measurements

EMI SE is attenuating ability of materials for incident EM waves, which is defined as the logarithmic ratio of incoming power (P_I) to transmitted power (P_T) as:

$$\text{SE (dB)} = 10 \log\left(\frac{P_I}{P_T}\right) \quad (1)$$

When incident EM waves arrive on shielding materials, they are reflected, absorbed, and/or transmitted. The reflection (R), absorption (A), and transmission (T) coefficients must add up to 1, that is,

$$R + A + T = 1 \quad (2)$$

The total EMI SE (SE_T) is the sum of contributions from reflection (SE_R), absorption (SE_A), and internal multiple reflections (SE_M). At higher EMI SE values than 15 dB, the contribution from internal multiple reflection is considered that is merged in the absorption. Thus, the SE_T can be written as:

$$SE_T = SE_R + SE_A \quad (3)$$

The absorbed EM waves in a material is related to effective absorption coefficient (A_{eff}), which can be described as:

$$A_{eff} = \frac{1 - R - T}{1 - R} \quad (4)$$

And the SE_T, SE_R, and SE_A are expressed in terms of transmission (T), reflection (R), and effective absorption (A_{eff}) coeffiecients as:

$$SE_T = 10 \log\left(\frac{1}{T}\right) \quad (5)$$

$$SE_R = 10 \log\left(\frac{1}{1 - R}\right) \quad (6)$$

$$SE_A = SE_T - SE_R = 10\log\left(\frac{1}{1 - A_{eff}}\right) = 10 \log\left(\frac{1 - R}{T}\right) \quad (7)$$

Note S2: Discussion on EMI shielding mechanism of materials

Some composites have higher SE_A than SE_R values despite high reflection coefficient (R). Although they are EM wave-reflecting material, they can be seen to accomplish EMI shielding through absorption with high SE_A value. For example, the Ni70 composite exhibited higher SE_A (76.4 dB) than SE_R (10.9 dB), while it showed lower absorption (A = 0.106) than reflection (R = 0.894), which means that the material absorbed only 10.6% of incident EM waves and reflected 89.4% of them. These confusing data comes from SE_A, which is calculated with the effective absorption coefficient (A_{eff}). The A represents the proportion of absorption for total amount of incident EM waves. On the other hand, the A_{eff} represents proportion of absorption for EM waves only inside a material that is not considering reflected EM waves on the surface of material. Hence, simple comparison of SE_A and SE_R cannot show the contribution of absorption and reflection, since EM wave-absorbing performance could be overestimated. Instead, for an absorption dominant EMI shielding material, its R and SE_R can be used as criteria, which should be less than 50% and 3.01 dB, respectively, as following process[44]:

$R = 0.5 = 50\%$ ($A \approx 0.5$, $T \approx 0$ for most EMI shielding materials)

$SE_R = -10 \log (1 - R) = -10 \log (1 - 0.5) = 3.01$ dB

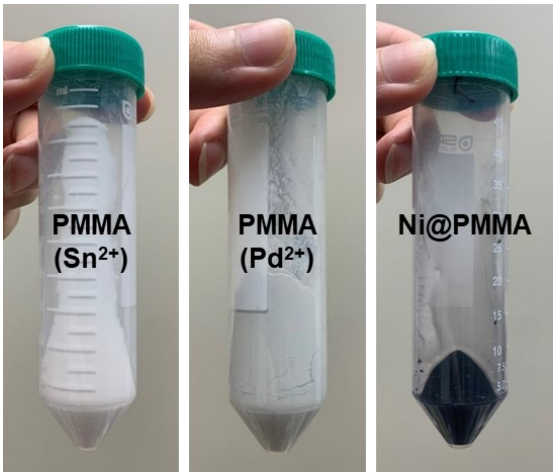

Fig. S13. Digital images of various microspheres in the fabrication process of nickel shells, showing different colors.

Supporting references

1 J. Ling, W. Zhai, W. Feng, B. Shen, J. Zhang and W. g. Zheng, *ACS Appl. Mater. Interfaces*, 2013, **5**, 2677–2684.

2 D.-X. Yan, P.-G. Ren, H. Pang, Q. Fu, M.-B. Yang and Z.-M. Li, *J. Mater. Chem.*, 2012, **22**, 18772–18774.

3 S.-T. Hsiao, C.-C. M. Ma, H.-W. Tien, W.-H. Liao, Y.-S. Wang, S.-M. Li and Y.-C. Huang, *Carbon*, 2013, **60**, 57–66.

4 S.-T. Hsiao, C.-C. M. Ma, W.-H. Liao, Y.-S. Wang, S.-M. Li, Y.-C. Huang, R.-B. Yang and W.-F. Liang, *ACS Appl. Mater. Interfaces*, 2014, **6**, 10667–10678.

5 D.-X. Yan, H. Pang, B. Li, R. Vajtai, L. Xu, P.-G. Ren, J.-H. Wang and Z.-M. Li, *Adv. Funct. Mater.*, 2015, **25**, 559–566.

6 N. Agnihotri, K. Chakrabarti and A. De, *RSC Adv.*, 2015, **5**, 43765–43771.

7 G. George, S. M. Simon, P. V. P, S. M. S, M. Faisal, R. Wilson, A. Chandran, B. P. R, C. Joseph and N. V. Unnikrishnan, *RSC Adv.*, 2018, **8**, 30412–30428.

8 H.-B. Zhang, Q. Yan, W.-G. Zheng, Z. He and Z.-Z. Yu, *ACS Appl. Mater. Interfaces*, 2011, **3**, 918–924.

9 Z. Chen, C. Xu, C. Ma, W. Ren and H.-M. Cheng, *Adv. Mater.*, 2013, **25**, 1296–1300.

10 F. Shahzad, S. Yu, P. Kumar, J.-W. Lee, Y.-H. Kim, S. M. Hong and C. M. Koo, *Compos. Struct.*, 2015, **133**, 1267–1275.

11 X.-H. Li, X. Li, K.-N. Liao, P. Min, T. Liu, A. Dasari and Z.-Z. Yu, *ACS Appl. Mater. Interfaces*, 2016, **8**, 33230–33239.

12 L. Kong, X. Yin, M. Han, X. Yuan, Z. Hou, F. Ye, L. Zhang, L. Cheng, Z. Xu and J. Huang, *Carbon*, 2017, **111**, 94–102.

13 Q. Wei, S. Pei, X. Qian, H. Liu, Z. Liu, W. Zhang, T. Zhou, Z. Zhang, X. Zhang, H.-M. Cheng and W. Ren, *Adv. Mater.*, 2020, **32**, 1907411.

14 T. Kuang, L. Chang, F. Chen, Y. Sheng, D. Fu and X. Peng, *Carbon*, 2016, **105**, 305–313.

15 M. Arjmand, M. Mahmoodi, G. A. Gelves, S. Park and U. Sundararaj, *Carbon*, 2011, **49**, 3430–3440.

16 M. H. Al-Saleh and U. Sundararaj, *Carbon*, 2009, **47**, 1738–1746.

17 Z. Zeng, H. Jin, M. Chen, W. Li, L. Zhou and Z. Zhang, *Adv. Funct. Mater.*, 2016, **26**, 303–310.

18 Y. Yang, M. C. Gupta, K. L. Dudley and R. W. Lawrence, *Nano Lett.*, 2005, **5**, 2131–2134.

19 N. Li, Y. Huang, F. Du, X. He, X. Lin, H. Gao, Y. Ma, F. Li, Y. Chen and P. C. Eklund, *Nano Lett.*, 2006, **6**, 1141–1145.

20 Y. Chen, H.-B. Zhang, Y. Yang, M. Wang, A. Cao and Z.-Z. Yu, *Adv. Funct. Mater.*, 2016, **26**, 447–455.

21 Z. Zeng, M. Chen, H. Jin, W. Li, X. Xue, L. Zhou, Y. Pei, H. Zhang and Z. Zhang, *Carbon*, 2016, **96**, 768–777.

22 M. Farukh, A. P. Singh and S. K. Dhawan, *Compos. Sci. Technol.*, 2015, **114**, 94–102.

23 A. Chaudhary, S. Kumari, R. Kumar, S. Teotia, B. P. Singh, A. P. Singh, S. K. Dhawan and S. R. Dhakate, *ACS Appl. Mater. Interfaces*, 2016, **8**, 10600–10608.

24 S. Kuester, C. Merlini, G. M. O. Barra, J. C. Ferreira, A. Lucas, A. C. de Souza and B. G. Soares, *Compos. B. Eng.*, 2016, **84**, 236–247.

25 X. Jiang, D.-X. Yan, Y. Bao, H. Pang, X. Ji and Z.-M. Li, *RSC Adv.*, 2015, **5**, 22587–22592.

26 V. K. Sachdev, K. Patel, S. Bhattacharya and R. P. Tandon, *J. Appl. Polym. Sci.*, 2011, **120**, 1100–1105.

27 M. H. Al-Saleh, W. H. Saadeh and U. Sundararaj, *Carbon*, 2013, **60**, 146–156.

28 A. Ameli, P. U. Jung and C. B. Park, *Carbon*, 2013, **60**, 379–391.

29 M. Crespo, N. Méndez, M. González, J. Baselga and J. Pozuelo, *Carbon*, 2014, **74**, 63–72.

30 M. Bayat, H. Yang, F. K. Ko, D. Michelson and A. Mei, *Polymer*, 2014, **55**, 936–943.

31 K. Yao, J. Gong, N. Tian, Y. Lin, X. Wen, Z. Jiang, H. Na and T. Tang, *RSC Adv.*, 2015, **5**, 31910–31919.

32 Y. Chen, Y. Wang, H.-B. Zhang, X. Li, C.-X. Gui and Z.-Z. Yu, *Carbon*, 2015, **82**, 67–76.

33 A. P. Singh, M. Mishra, P. Sambyal, B. K. Gupta, B. P. Singh, A. Chandra and S. K. Dhawan, *J. Mater. Chem. A*, 2014, **2**, 3581–3593.

34 M. Arjmand, A. A. Moud, Y. Li and U. Sundararaj, *RSC Adv.*, 2015, **5**, 56590–56598.

35 M. H. Al-Saleh, G. A. Gelves and U. Sundararaj, *Compos. Part A Appl. Sci. Manuf.*, 2011, **42**, 92–97.

36 X. Shui and D. D. L. Chung, *J. Electron. Mater.*, 1997, **26**, 928–934.

37 F. Fang, Y.-Q. Li, H.-M. Xiao, N. Hu and S.-Y. Fu, *J. Mater. Chem. C*, 2016, **4**, 4193–4203.

38 A. A. Al-Ghamdi and F. El-Tantawy, *Compos. Part A Appl. Sci. Manuf.*, 2010, **41**, 1693–1701.

39 R. Sun, H.-B. Zhang, J. Liu, X. Xie, R. Yang, Y. Li, S. Hong and Z.-Z. Yu, *Adv. Funct. Mater.*, 2017, **27**, 1702807.

40 F. Shahzad, M. Alhabeb, C. B. Hatter, B. Anasori, S. Man Hong, C. M. Koo and Y. Gogotsi, *Science*, 2016, **353**, 1137.

41 M. Han, X. Yin, H. Wu, Z. Hou, C. Song, X. Li, L. Zhang and L. Cheng, *ACS Appl. Mater. Interfaces*, 2016, **8**, 21011–21019.

42 S. Zhao, H.-B. Zhang, J.-Q. Luo, Q.-W. Wang, B. Xu, S. Hong and Z.-Z. Yu, *ACS Nano*, 2018, **12**, 11193–11202.

43 B.-W. Li, Y. Shen, Z.-X. Yue and C.-W. Nan, *Appl. Phys. Lett.*, 2006, **89**, 132504.

44 U. Hwang, J. Kim, M. Seol, B. Lee, I.-K. Park, J. Suhr and J.-D. Nam, *ACS Omega*, 2022, **7**, 4135-4139.